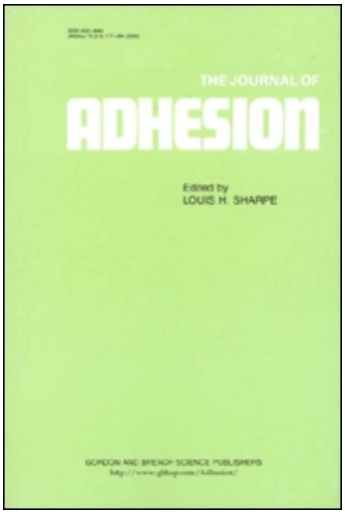

The Journal of Adhesion
Publication details, including instructions for authors and subscription information:
http://www.informaworld.com/smpp/title~content=t713453635

Strength of adhesive joints with adherend yielding: I. Analytical model

R. X. Wang[a]; J. Cui[a]; A. N. Sinclair[a]; J. K. Spelt[a]
[a] Department of Mechanical and Industrial Engineering, University of Toronto, Toronto, Ontario, Canada

Online publication date: 08 September 2010

To cite this Article Wang, R. X. , Cui, J. , Sinclair, A. N. and Spelt, J. K.(2003) 'Strength of adhesive joints with adherend yielding: I. Analytical model', The Journal of Adhesion, 79: 1, 23 — 48
To link to this Article: DOI: 10.1080/00218460309561
URL: http://dx.doi.org/10.1080/00218460309561

The Journal of Adhesion, 79: 23–48, 2003

0021-8464/03 $12.00 +.00
DOI: 10.1080/00218460390147933

Taylor & Francis
Taylor & Francis Group

STRENGTH OF ADHESIVE JOINTS WITH ADHEREND YIELDING: I. ANALYTICAL MODEL

R. X. Wang
J. Cui
A. N. Sinclair
J. K. Spelt
Department of Mechanical and Industrial Engineering,
University of Toronto, Toronto, Ontario, Canada

A sandwich element can be isolated in all two-dimensional adhesive joints, thereby simplifying the analysis of strain and stress. An adhesive sandwich model has been developed that accommodates arbitrary loading, a bilinear adherend stress-strain response, and any form of nonlinear adhesive behavior. The model accounts for both the bending deformation and the shear deformation of the adherends. Stress and strain distributions in the adhesive were obtained by solving a system of six differential equations using a finite-difference method. For a sample adhesive sandwich, the adhesive strains and stresses from the new model were compared with those of other models. Finally, the model was coupled with an analytical solution for the detached section of an adhesive joint in peel. The stress and strain distributions in the adhesive and the root curvature of the peel adherend were then compared with finite element results. An accompanying article in this issue uses the model with experimental peel data to investigate the suitability of various adhesive failure criteria.

Keywords: Peel; Adhesive; Strength; Adherend yielding; Sandwich model

Received 20 March 2002; in final form 8 July 2002.

The work was supported by the Centre for Automotive Materials and Manufacturing. The support of Essex Specialty Products Inc., Henkel Corp., and Alcan International Ltd. is gratefully acknowledged.

Address correspondence to J. K. Spelt, Department of Mechanical and Industrial Engineering, University of Toronto, 5 King's College Road, Toronto, Ontario, Canada M5S 3G8. E-mail: spelt@mie.utoronto.ca

INTRODUCTION

The wider use of adhesives in structural applications requires the development of procedures for the prediction of joint strength. In cases where the adherends remain elastic up to joint failure, the ultimate fracture loads for many joint geometries can be predicted using a critical energy release rate that is a function of the mode ratio of loading [1, 2]. Similar capabilities do not exist; for adhesive joints in which large-scale adherend yielding occurs prior to adhesive failure as, for example, when bonded metal sheets in automotive structures collapse under impact. This situation is complicated by the varying degree of constraint imposed on the adhesive failure zone (crack tip if using a fracture model) by the yielding adherends. For example, a relatively high degree of stress concentration will exist in the adhesive at the end of the bonded region if the adherend properties (thickness, yield strength), loading direction and magnitude, and adhesive strength combine to produce a small radius of curvature. At the other extreme, the elastic arms of a double cantilever beam specimen, for example, will create a relatively large three-dimensional loading zone in the adhesive, thereby increasing the volume of material involved in the yielding and fracture process. Experience has shown that, with elastic adherends, the size and nature of the loading zone is adequately correlated with the mode ratio alone [3]. This may not be the case with adherends that undergo extensive yielding, and it may be necessary to have an additional parameter characterizing the degree of stress concentration in the adhesive layer.

Crocombe and Bigwood [4] developed an innovative "adhesive sandwich" model that accommodates the nonlinear stress-strain response of both the adhesive and the adherends subject to arbitrary loads imposed on the ends of the sandwich element. Such a generic sandwich model can be incorporated into a wide variety of common adhesive joint geometries. The adhesive was assumed to behave as a series of nonlinear shear and tensile springs coupled by the von Mises yielding criterion. This model resulted in a set of six nonlinear first-order differential equations that were solved numerically using a finite-difference method. The sandwich model produced reasonable agreement with a finite element model.

In the present work, the adhesive sandwich model of Crocombe and Bigwood [4] was first extended to include shear deformation of the adherends. The model was then coupled to an existing analytical model for the detached adherend in a peel specimen, thereby allowing for the investigation of two failure criteria using peel test data described in the accompanying article in this volume [5]. The ultimate

objective is to develop a means of predicting adhesive failure in arbitrary joints subject to large-scale adherend yielding. In the general case, the reactions acting on the adhesive sandwich might be supplied by a finite element or other structural model, rather than by the specialized model of a detached peel strip used here.

SANDWICH MODEL

For any two-dimensional adhesive joint geometry, an adhesive sandwich element can be isolated as shown in Figure 1. Both adherends are treated as beams subject to arbitrary bending (M), tensile (T), or shear (V) loads. Figure 2 shows the free-body diagrams for the adherends over a differential length dx of the sandwich. The development of the sandwich model is presented below in two sections: (1) the analysis of the nonlinear adhesive behavior and (2) adherend modeling. Only the modifications that were made to the original Crocombe and Bigwood model [4] are discussed in detail. These include the following:

1. Adherend shear deformation is considered. This contributes to earlier yielding and larger adherend curvatures than predicted by the original model [4].
2. The present model was used to investigate several stress states in the adhesive:

    a. plane strain ($\varepsilon_z = 0$) and plane stress ($\sigma_z = 0$) both with no tensile stress in the x direction ($\sigma_x = 0$)
    b. uniaxial strain ($\varepsilon_x = \varepsilon_z = 0$), thereby generating a finite σ_x. Only the plane strain condition ($\varepsilon_z = 0$) was studied in Crocombe and Bigwood [4], and it was assumed that $\sigma_x = 0$.

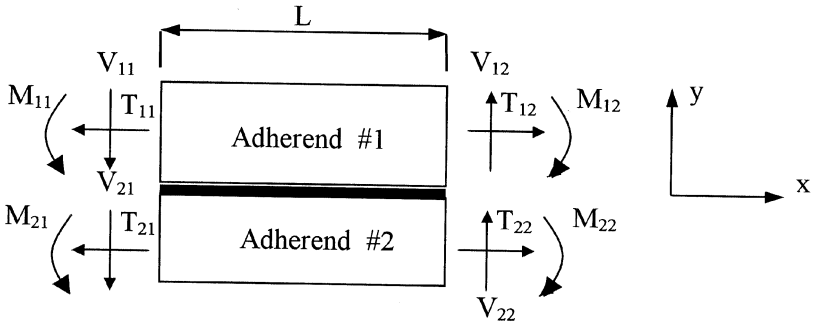

FIGURE 1 A general adhesive sandwich element subject to arbitrary end loads as found in many typical joints.

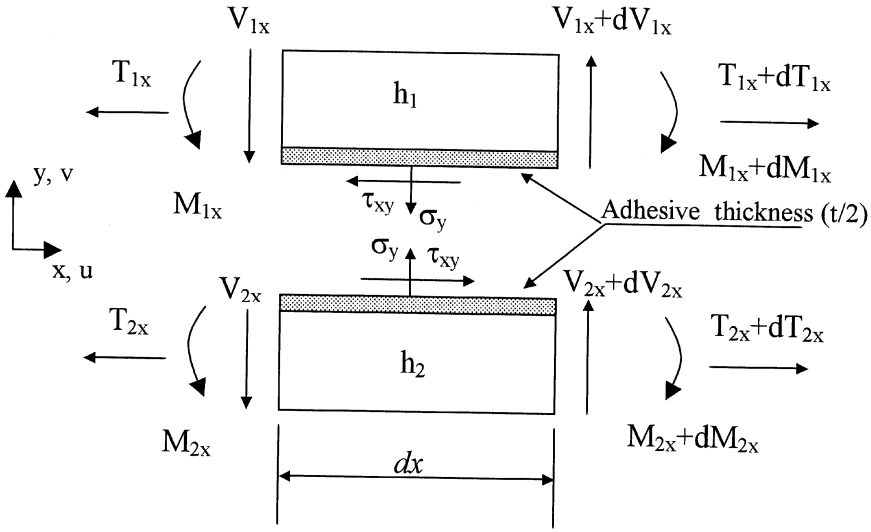

FIGURE 2 A free-body diagram of the adherends over a differential length dx of an adhesive sandwich.

Governing Equations

Under the assumption of a uniaxial strain in the adhesive layer ($\varepsilon_x = \varepsilon_z = 0$) and plane strain adherends ($\varepsilon_z = 0$), and following an approach similar to Crocombe and Bigwood [4], the equations governing the equilibrium of the adherends (Figure 2) are formulated as:

$$\frac{dT_{1x}}{dx} = \frac{E_s \gamma}{2(1+\upsilon_p)} \tag{1a}$$

$$\frac{dV_{1x}}{dx} = \frac{E_s \varepsilon}{(\upsilon_p - 1 + 2\upsilon_p^2)}\left(\upsilon_p - 1\right) \tag{1b}$$

$$\frac{dM_{1x}}{dx} = V_{1x} - \frac{(h_1 + t)E_s}{4(1+\upsilon_p)}\gamma \tag{1c}$$

$$\frac{d\gamma}{dx} = \left\{K_{1x}^{T,M}(-h_1/2 + e_1) - K_{2x}^{T,M}(h_2/2 + e_2)\right\}\Big/ t \tag{1d}$$

$$\frac{d\varepsilon}{dx} = C \tag{1e}$$

$$\frac{dC}{dx} = (K_{2x} - K_{1x})/t \tag{1f}$$

where T_{1x}, V_{1x}, M_{1x}, γ, ε, and C are six unknowns; K_{1x} and K_{2x} are the total curvatures for adherend 1 and adherend 2, respectively, while $K_{1x}^{T,M}$ and $K_{2x}^{T,M}$ are curvatures due to T and M loads only. E_s is the secant modulus of the nonlinear adhesive, defined later in Equation (6); e_1 and e_2 are the offsets of the neutral axis due to tensile force in adherends 1 and 2, respectively; and υ_p is the plastic Poisson ratio of the adhesive. The curvature terms are implicit functions of the respective adherend local reactions (T, V, M), *i.e.*,

$$K_{1x} = f_1(T_{1x},\ V_{1x},\ M_{1x}),\ K_{1x}^{T,M} = f_2(T_{1x},\ M_{1x}),$$
$$K_{2x} = f_3(T_{1x},\ V_{1x},\ M_{1x}), K_{2x}^{T,M} = f_4(T_{1x},\ M_{1x}).$$

The local loads (T_{2x}, V_{2x}, M_{2x}) for adherend 2 can always be derived by an overall force balance:

$$T_{2x} = T_{11} + T_{21} - T_{1x} \tag{2}$$

$$V_{2x} = V_{11} + V_{21} - V_{1x} \tag{3}$$

$$M_{2x} = (M_{11} + M_{21}) - M_{1x} + (V_{11} + V_{21})x + (T_{11} - T_{1x})h' \tag{4}$$

where h' is defined as

$$h' = \frac{2t + h_1 + h_2}{2} \tag{5}$$

Therefore, K_{2x} and $K_{2x}^{T,M}$ can always be interpreted as a function of T_{1x}, V_{1x}, and M_{1x}.

Adhesive Model

The adhesive layer is modeled as a set of nonlinear shear and tension springs coupled by the von Mises yielding criterion. The uniaxial tensile stress-strain curve for the adhesive can be defined using either an equation or a series of data interpolated using a spline fit, as shown in Figure 3. Adhesive plasticity is treated using an equivalent instantaneous modulus, the secant modulus, as shown in Figure 3, and is defined as

$$E_s = \frac{\sigma_e}{\varepsilon_e} \tag{6}$$

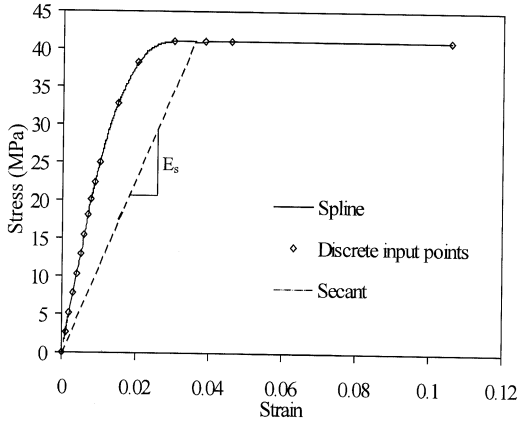

FIGURE 3 Spline interpolation of discrete uniaxial stress and strain data for adhesive and illustration of secant modulus.

where σ_e is the adhesive von Mises stress which can be calculated for the uniaxial strain adhesive model ($\varepsilon_z = \varepsilon_x = 0$) in terms of the component stresses (σ_y and τ_{xy}) as

$$\sigma_e = \left\{ \left(1 - \frac{\upsilon_p}{1 - \upsilon_p} \right)^2 \sigma_y^2 + 3\tau_{xy}^2 \right\}^{0.5} \tag{7}$$

The corresponding von Mises strain, ε_e, can be found by combining Equations (6) and (7) using the secant modulus formulation of Hooke's law to give $\sigma_y = \frac{1-\upsilon_p}{1-\upsilon_p-2\upsilon_p^2} E_s \varepsilon_y$ and $\tau_{xy} = \frac{E_s}{2(1+\upsilon_p)} \gamma_{xy}$:

$$\varepsilon_e = \left\{ \frac{\left(1 - 2\upsilon_p\right)^2}{\left(\upsilon_p - 1 + 2\upsilon_p^2\right)^2} \varepsilon^2 + \frac{0.75\gamma^2}{\left(1 + \upsilon_p\right)^2} \right\}^{0.5} \tag{8}$$

where the plastic Poisson ratio υ_p for the adhesive is

$$\upsilon_p = \frac{1}{2} \left[1 - \frac{E_s}{E} (1 - 2\upsilon) \right] \tag{9}$$

with υ being the elastic adhesive Poisson ratio. Although υ_p should depend on the state of stress, a constant value of 0.47 was used for the adhesive. The work of Crocombe and Bigwood [4] showed this to be an acceptable approximation.

Adherend Model

The adherends of the sandwich element (Figure 2) are modeled as beams having a bilinear stress-strain response. Since the analysis can be applied to both the upper and lower adherends, the subscripts 1 and 2 are omitted in this section for clarity.

The von Mises yield response of the bilinear adherend, as illustrated in Figure 4, is described by:

$$\sigma_e = \begin{cases} E_{el}\varepsilon_e & \varepsilon_e \le \varepsilon_{yp} \\ \sigma_{yp} + E_{pl}(\varepsilon_e - \varepsilon_{yp}) & \varepsilon_e > \varepsilon_{yp} \end{cases} \tag{10}$$

where $\sigma_{yp} = E_{el}\varepsilon_{yp}$ and $E_{pl} = \alpha E_{el}$, with α a constant.

The analysis of the tensile stress distribution (σ_x) across the thickness of the adherends due to local bending moment (M) and axial force (T) is facilitated using the concept of longitudinal stress and strain [4]. Figure 4 shows the von Mises $\sigma_e - \varepsilon_e$ curve, which is equivalent to the uniaxial stress-strain curve for the adherends. The "Longitudinal #1" curve is a calculated x-direction longitudinal $\sigma_x - \varepsilon_x$ response of the adherends under plane strain conditions ($\varepsilon_z = 0$) based on the given $\sigma_e - \varepsilon_e$ curve. In this case, the adherend shear stress τ_{xy} due to V is neglected. This is the case Crocombe and Bigwood used in their analysis [4] by applying the following equations:

$$\sigma_x = E_{el}\frac{\varepsilon_x}{1 - \upsilon_p^2} \qquad \text{if } \varepsilon_x \ge \varepsilon_{yp} \tag{11}$$

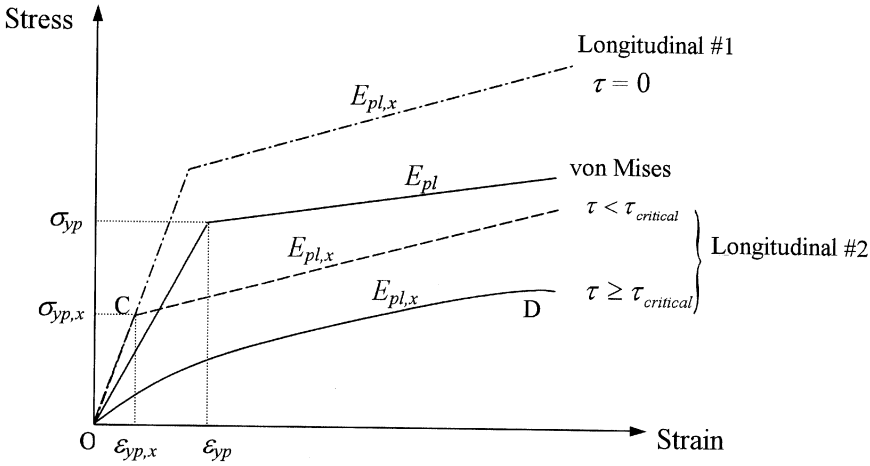

FIGURE 4 Bilinear plane strain approximation of von Mises and longitudinal and stress-strain response for the adherends.

$$\sigma_x = \sigma_{yp} + E_{pl}\frac{\varepsilon_x - \varepsilon_{yp}}{1-\upsilon_p^2} \qquad \text{if } \varepsilon_x > \varepsilon_{yp} \tag{12}$$

The present model takes the shear stress τ_{xy} into account, therefore the longitudinal $\sigma_x - \varepsilon_x$ response is transformed into the "Longitudinal #2" response in Figure 4. This can be further classified as bilinear and nonlinear under two situations, depending on the value of the average shear stress τ across the thickness of the adherends: $\tau < \tau_{critical}$ and when $\tau \geq \tau_{critical}$, where $\tau_{critical} = \frac{\sigma_{yp}}{\sqrt{3}}$.

If $\tau < \tau_{critical}$, then for both the linear elastic (O–C) and plastic (C–C′) stages, the longitudinal adherend stress σ_x can be calculated by [6]

$$\sigma_x = \frac{\left\{E_{el}^2\left[\frac{\left(1-\upsilon_p+\upsilon_p^2\right)}{\left(1-\upsilon_p^2\right)^2}\varepsilon_x^2 + \frac{3}{4}\frac{\left(1-\upsilon_p\right)^2}{\left(1-\upsilon_p^2\right)^2}\gamma^2\right] - 3\tau^2\right\}^{\frac{1}{2}}}{\left(1-\upsilon_p+\upsilon_p^2\right)^{\frac{1}{2}}} \qquad \text{if } \varepsilon_x \leq \varepsilon_{yp,x} \tag{13a}$$

$$\sigma_x = \frac{\left\{\left[\sigma_{yp} + E_{pl}\left[\frac{\left(1-\upsilon_p+\upsilon_p^2\right)}{\left(1-\upsilon_p^2\right)^2}\varepsilon_x^2 + \frac{3}{4}\frac{\left(1-\upsilon_p\right)^2}{\left(1-\upsilon_p^2\right)^2}\gamma^2\right]^{\frac{1}{2}} - E_{pl}\varepsilon_{yp}\right]^2 - 3\tau^2\right\}^{\frac{1}{2}}}{\left(1-\upsilon_p+\upsilon_p^2\right)^{\frac{1}{2}}} \quad \text{if } \varepsilon_x > \varepsilon_{yp,x} \tag{13b}$$

where $\varepsilon_{yp,x}$ is the yield strain corresponding to the bilinear longitudinal $\sigma_x - \varepsilon_x$ curve (Longitudinal 2, $\tau < \tau_{critical}$, Figure 4). The corresponding adherend shear strain is given by

$$\gamma = \begin{cases} \frac{2\tau(1+\upsilon_e)}{E_{el}} & \tau \leq \tau_{critical} \\ \frac{2\tau_{critical}(1+\upsilon_e)}{E_{el}} + \frac{2(\tau-\tau_{critical})\left(1+\upsilon_p\right)}{E_{pl}} & \tau > \tau_{critical} \end{cases} \tag{14}$$

where υ_e and υ_p are the adherend elastic and plastic Poisson ratio, respectively.

The differentiation of σ_x with respect to ε_x gives the corresponding longitudinal Young's modulus for both the linear elastic stage, *i.e.*, Equation (15), and for the nonlinear plastic stage, which can be approximated as Equation (16):

$$E_{el,x} = \frac{E_{el}}{\left(1-\upsilon_p^2\right)} \qquad \text{if } \varepsilon_x \leq \varepsilon_{yp,x} \tag{15}$$

$$E_{pl,x} \approx \frac{E_{pl}}{\left(1-\upsilon_p^2\right)} \qquad \text{if } \varepsilon_x > \varepsilon_{yp,x} \tag{16}$$

where the longitudinal yielding strain $\varepsilon_{yp,x}$ is given by

$$\varepsilon_{yp,x} = \frac{\left(1-\upsilon_p^2\right)}{\left(1-\upsilon_p+\upsilon_p^2\right)^{\frac{1}{2}}}\left[\varepsilon_{yp}^2 - \frac{3}{4}\frac{1}{\left(1+\upsilon_p\right)^2}\gamma^2\right]^{\frac{1}{2}} \tag{17}$$

If $\tau \geq \tau_{critical}$, then it effectively means $\varepsilon_{yp,x} = 0$, and any loading of either tensile (T) or bending (M) will lead the adherend immediately into the nonlinear yielding stage, shown as the curve "O-D" in Figure 4. In this case, the corresponding longitudinal Young's modulus is obtained from Equation (13b) using the secant modulus approach of Equation (6) as

$$E_{pl,x} = \frac{\sigma_x}{\varepsilon_x} = \frac{\left\{\left[\sigma_{yp} + E_{pl}\left[\frac{\left(1-\upsilon_p+\upsilon_p^2\right)}{\left(1-\upsilon_p^2\right)^2}\varepsilon_x^2 + \frac{3}{4}\frac{\left(1-\upsilon_p\right)^2}{\left(1-\upsilon_p^2\right)^2}\gamma^2\right]^{\frac{1}{2}} - E_{pl}\varepsilon_{yp}\right]^2 - 3\tau^2\right\}^{\frac{1}{2}}}{\varepsilon_x\left(1-\upsilon_p+\upsilon_p^2\right)^{\frac{1}{2}}} \tag{18}$$

Corresponding to this case, a special adherend load category (named #5) will be discussed in a later section, to be used in addition to the four categories presented in Crocombe and Bigwood [4].

Bilinear Adherend Beam Analysis

This section considers the calculation of the adherend curvatures $K_{1x}, K_{1x}^{T,M}, K_{2x}$, and $K_{2x}^{T,M}$, and the neutral axis offsets e_1 and e_2 using plate bending theory. For clarity, the x subscript and the adherend designations 1 and 2 are omitted in this section. Before moving on to the analysis, the total adherend curvature and its components due to bending and shear force will be addressed.

1. Total Adherend Curvature, K

The total curvature is obtained as

$$K = K^{T,M} + K^V \tag{19}$$

where $K^{T,M}$ is the adherend curvature due to the bending moment (M) and the tensile force (T) acting at the section, while K^V is the curvature due to the shear force (V) acting at the section.

2. Bending Curvature $K^{T,M}$

The determination of tensile stress (σ_x) requires the application of the bilinear longitudinal $\sigma_x - \varepsilon_x$ response derived above. The longitudinal properties such as elastic Young's modulus $E_{el,x}$, plastic Young's modulus $E_{yp,x}$, yielding strain $\varepsilon_{yp,x}$, and yielding stress $\sigma_{yp,x}$ were already defined in Equations (15) to (18). The longitudinal strain ε_x across the thickness of the adherends is assumed to vary linearly with the distance from the neutral axis. At a general distance y from the neutral axis, the longitudinal tensile stress σ_x is calculated by

$$\sigma_x = \begin{cases} \sigma_{yp,x} + E_{pl,x}K_{M,T}(y-r) = \sigma_{yp,x} + \alpha\sigma_{yp,x}(y-r)/r & y \geq r \\ \sigma_{yp,\,x}y/r & y \leq r \end{cases} \quad (20)$$

where α is defined as in Equation (10) as the ratio of the adherend plastic and elastic moduli (E_{pl}/E_{el}), and r is the "elastic semidepth," defined below in Equation (22) as the distance from the neutral axis to the point where yield would begin (this point may be outside the beam).

Five categories of adherend stress (σ_x) distribution may occur according to the values of the moment M, tensile force T, and shear force V. Categories 1 to 4 are similar to those in the Crocombe and Bigwood analysis [4] except that the calculation of longitudinal stress-strain response properties (*i.e.*, $\sigma_{yp,x}$ and $\varepsilon_{yp,x}$) is different due to the inclusion of shear stress, as mentioned above. For each category, the σ_x distribution is determined using the simultaneous solution of the following equilibrium equations for the local moment (M) and tension (T) per unit adherend width:

$$T = \int_{-h/2}^{h/2} \sigma_x dy \quad \text{and} \quad M = \int_{-h/2}^{h/2} y\sigma_x \, dy \quad (21)$$

At a distance r (elastic semidepth) from the neutral axis, the strain ε_x reaches the yielding strain $\varepsilon_{yp,x}$, and the value of r can be related to the adherend bending curvature $K^{T,M}$ as

$$K^{T,M} = \frac{\varepsilon_{yp,x}}{r} = \frac{1}{r}\frac{\sigma_{yp,x}}{E_{el,x}} \quad (22)$$

The actual neutral axis under this general loading that includes tension is located a distance e from the neutral axis due to bending alone.

However, for category #5, the following equations are used to calculate $K^{T,M}$ and e directly:

$$e = \frac{Th^2}{12M}, \quad K^{T,M} = \frac{\sigma_{yp,x}}{rE_{pl,x}}, \quad r = \frac{\sigma_{yp,x}h^3}{12M} \tag{23}$$

The method of determining which category will apply during the problem solution is similar to that in Crocombe and Bigwood [4]. Category #5 applies only when $\tau \geq \tau_{critical}$, where τ is the average shear stress across the adherend.

3. Shear Curvature K^V

The calculation of the shear curvature K^V due to the shear force acting at the section requires a known shear stress distribution across the section. An assumption is made here to simplify the analysis [7]:

$$K^V = \frac{d^2u_V}{d^2x} = \frac{d\gamma_{neutral}}{dx} = \frac{1}{G}\frac{d\tau_{neutral}}{dx} \tag{24}$$

where u_V is the vertical deflection of the adherend due to shear force, and G, $\gamma_{neutral}$, and $\tau_{neutral}$ are the shear modulus, shear strain, and shear stress, respectively, at the centroid of the adherend.

The derivation of $\tau_{neutral}$ is described in the Appendix. It is given by

$$\tau_{neutral} = \begin{cases} -AV + \frac{1}{2}\tau_a & M \leq M_{critical} \\ -BV + \frac{1}{2}\tau_a & M > M_{critical} \end{cases} \tag{25}$$

where $A = \frac{3}{2bh}$, $B = \frac{\left[12(1-\alpha)+3\alpha h^2/r^2\right]}{16r(1-\alpha)+2\alpha h^3/r^2}$, and τ_a is the shear stress applied to the adherend by the adhesive. Differentiation with respect to x gives

$$\frac{d\tau_{neutral}}{dx} = \begin{cases} -A\sigma + \frac{1}{2}\frac{d\tau_a}{dx} & M \leq M_{critical} \\ -B\sigma + \frac{1}{2}\frac{d\tau_a}{dx} & M > M_{critical} \end{cases} \tag{26}$$

where $\frac{d\tau_a}{dx}$ is given by

$$\begin{aligned} \frac{d\tau_a}{dx} = G_S^{ads}\frac{d\gamma}{dx} &= \frac{E_S}{2t(1+\upsilon_p)}\left(\frac{du_1}{dx} - \frac{du_2}{dx}\right) \\ &= \frac{E_S}{2t(1+\upsilon_p)}\left\{\left[-K_{1x}^{T,M}\frac{h_1}{2} + \frac{T_{1x}\left(1-\upsilon_{1p}^2\right)}{E_S^{adh1}h_1}\right]\right. \\ &\quad \left. - \left[K_{2x}^{T,M}\frac{h_2}{2} + \frac{T_{2x}\left(1-\upsilon_{2p}^2\right)}{E_S^{adh2}h_2}\right]\right\} \end{aligned} \tag{27}$$

where E_s is the adhesive secant modulus (Equation (6)); E_s^{adh1} and E_s^{adh2} are the local secant Young's moduli of adherend 1 and 2, respectively, at the interfaces with the adhesive; υ_{1p} and υ_{2p} are the plastic Poisson ratio of adherend 1 and 2; and G_s^{ads} is the secant shear modulus of the adhesive, conceptually equivalent to E_s.

Substituting into Equation (26), the shear curvature of each adherend is given by

$$K^V = \frac{2E_S}{E_S^{adh}}\left[\frac{1}{4t}\left\{\left[-K_{1x}^{T,M}\frac{h_1}{2}+\frac{T_{1x}\left(1-\upsilon_{1p}^2\right)}{E_S^{adh1}h_1}\right]-\left[K_{2x}^{T,M}\frac{h_2}{2}+\frac{T_{2x}\left(1-\upsilon_{2p}^2\right)}{E_S^{adh2}h_2}\right]\right\}-D\frac{\varepsilon}{\left(1-\upsilon_p\right)}\right] \quad (28)$$

where $D = A$ if $M < M_{critical}$, and $D = B$ if $M \geq M_{critical}$.

Numerical Solution

Solving this system of six nonlinear first-order differential equations, Equations (1a–f) for the vector of unknowns $Y = [T_{1x}, V_{1x}, M_{1x}, \gamma, \varepsilon, C]^T$, is complicated by the associated auxiliary equations that require the solution of a set of nonlinear equations to find $K_{1x}, K_{1x}^{T,M}, K_{2x}, K_{2x}^{T,M}, e_1$, and e_2 under different categories. At each end of the sandwich, $x = 0, L$, six boundary values are specified for the elements of Y. After some unsuccessful attempts to employ a "shooting method" of solution in which the boundary value problem is treated as an initial value problem, a finite difference method [8, 9] was employed, using a solver (DBVFPD; Double (Precision) Boundary Value Problem Finite Difference) from the IMSL (International Mathematical and Statistical Library) Fortran library [10]. This is an adaptive finite difference program for first-order, nonlinear, ordinary boundary problems similar to the one used in Crocombe and Bigwood [4].

Implementation of DBVFPD Solver

The DBVFPD solver requires the introduction of a linearizing parameter *eps* to be embedded into the original differential equations such that when $eps = 0$, they become linear. Gradually raising the value of *eps* to 1 increases the degree of nonlinearity until the actual problem is obtained. In Equations (1a–f), parameters such as $E_s, K_{1x}, K_{1x}^{T,M}$, $K_{2x}, K_{2x}^{T,M}, e_1$, and e_2 are all nonlinear factors with implicit and

complicated expressions. When $eps = 0$ at the beginning of the solution procedure, they take on values corresponding to the purely elastic case.

In the finite difference technique, a mesh is defined over the region of interest as a series of points on which the set of differential equations are discretized and transformed into linear algebraic equations. The IMSL routine DBVFPD executes this meshing, the formulation of discrete equations, convergence testing, system solution, and subsequent mesh refinement.

To begin the calculation, the geometry of the joint and the material properties of both adhesive and adherends are input. The initial mesh grids and guess values for unknown variables are provided in compliance with the prescribed boundary conditions. Given the robustness of the DBVFPD solver in these types of problems, the initial guess values can be very approximate. For example, linear interpolation between the boundary values can be used for the guess values at all initial mesh grid points. The boundary conditions can be different from one case to another. They can be prescribed loads acting anywhere on the adherends of the joint, or they can be prescribed strains in the adhesive layer at the ends or somewhere along the overlap of the sandwich.

Comparisons with Other Models

The present sandwich model was compared with the model of Crocombe and Bigwood [4] and a finite element model [11] using the sandwich geometry and properties specified in Crocombe and Bigwood [4] and reproduced in Figure 5. Note that this sandwich is subject only to bending loads and is, therefore, not representative of the situation in a peel specimen. The adherend was assumed to have a bilinear stress-strain response, and the adhesive was described using the Prager formula:

$$\sigma_e = A \tan h \left\lfloor (E_{el} - E_{pl})\varepsilon_e / A \right\rfloor + E_{pl}\varepsilon_e \tag{29}$$

where A is the stress asymptote of the curve, E_{el} is the elastic Young's modulus, and E_{pl} is the plastic Young's modulus. The two-dimensional finite element model (ANSYS v. 5.7) used four layers of 4-node quadrilateral elements, 0.1 mm wide, through the adhesive thickness and five layers through each adherend.

Figure 6 shows the adhesive strains for these three models as a function of the distance from the left end of the sandwich of Figure 5. The peel strain here is the tensile strain normal to the adherend bonded surfaces, and all models assumed plane strain ($\varepsilon_z = 0$). As the

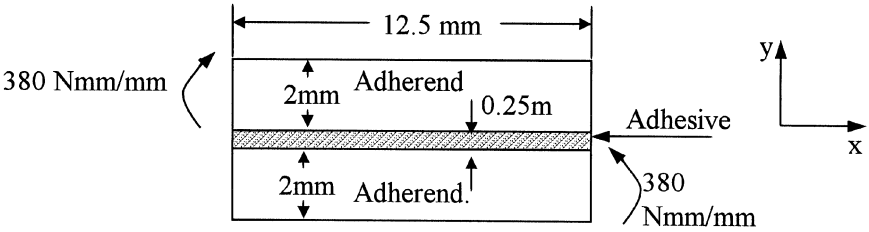

FIGURE 5 Adhesive sandwich element used to evaluate model. Adherend parameters: $E_{el} = 70\,\text{Gpa}$, $E_{pl} = 2\,\text{Gpa}$, $\sigma_{yp} = 300\,\text{Mpa}$; Adhesive parameters: $E_{el} = 5.74\,\text{Gpa}$, $E_{pl} = 408\,\text{Mpa}$, $A = 63\,\text{Mpa}$.

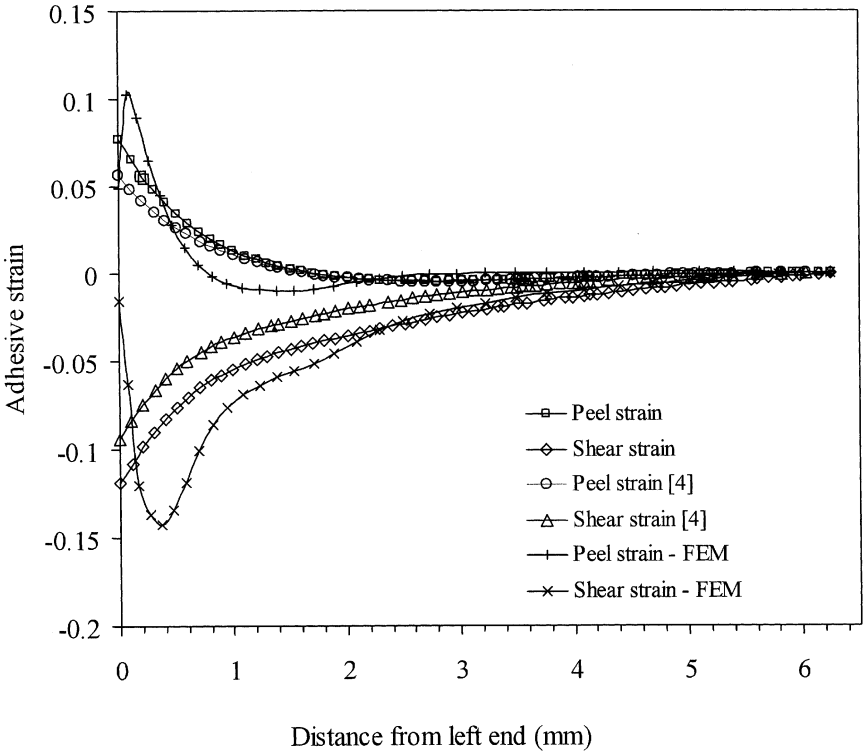

FIGURE 6 Adhesive peel and shear strains in sandwich of Figure 5 for present model, model of Crocombe and Bigwood [4] and FE model.

strain distributions are symmetric about the center of the joint, they are shown for only half of the joint overlap. The finite element data are taken from the nodes at the center line of the adhesive layer. It is seen that the overall trends of both the present model ($\varepsilon_z = 0$) and the original model [4] agree with the finite element result, except near the end of the joint where the finite element strains reach an extremum close to the free edge of the adhesive layer. Both the present modified model and the original model [4] fail to show this local maximum. As recognized in Crocombe and Bigwood [4], this is due to the finite element model capturing three effects that the analytical models miss: the large strain variation across the adhesive layer due to the square edge, the absence of shear stress at the free surface, and the finite adhesive longitudinal stress (σ_x). Since σ_x in the adhesive is tensile near the end of the overlap, by neglecting it both analytical models tend to predict a premature yielding of the adhesive, thereby contributing to a generally lower peel strain in this region. Comparing the present model with that of Crocombe and Bigwood [4], it is seen that the inclusion of shear deformation in the adherends has the effect of increasing curvature and hence the absolute magnitudes of both the peel and shear strains. This effect would be larger if the sandwich loading (Figure 5) included shear forces as in the case of a peel specimen.

The adhesive peel and shear stress distributions in the sandwich of Figure 5 are shown in Figure 7a. As expected from Figure 6, the inclusion of adherend shear deformation increases the absolute magnitude of the stresses near the end of the sandwich relative to the original model [4]. The finite element model predicts a relatively large maximum peel stress 0.2 mm from the end of the sandwich, but agrees well with the analytical models at the free surface.

The above two analytical models both assumed that $\sigma_x = 0$ in the adhesive layer. The consequences of this were examined in a simplified way by altering the present model so that $\varepsilon_x = \varepsilon_z = 0$ in the adhesive while retaining plane strain adherends (only $\varepsilon_z = 0$), thereby generating a finite adhesive σ_x (the uniaxial strain model). Figure 7b shows the von Mises stress distribution in the sandwich of Figure 5 for the present model and that of Crocombe and Bigwood [4] under the plane strain ($\varepsilon_z = 0$) assumption, the uniaxial strain assumption for the adhesive ($\varepsilon_x = \varepsilon_z = 0$), and the finite element model which assumed $\varepsilon_z = 0$ for both the adhesive and the adherends. It is seen that, in the region close to the edge, the two plane strain models gave results closer to the FEM than the uniaxial strain model, which predicted a flatter von Mises stress distribution. However, Figure 7c shows that the von

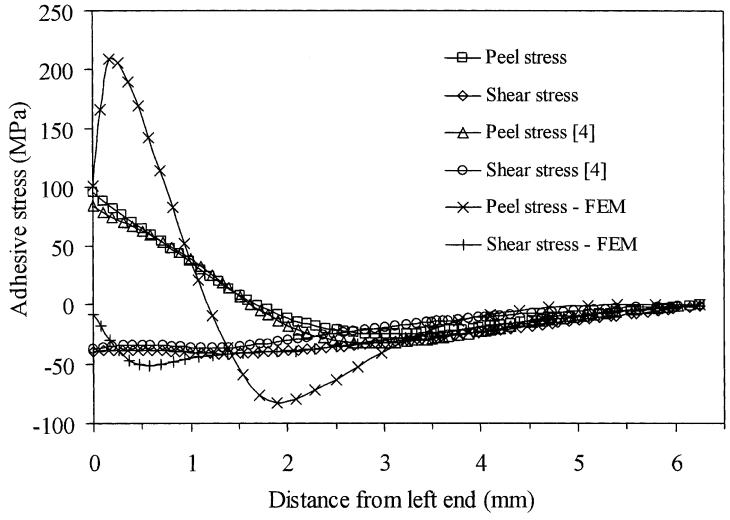

(a)

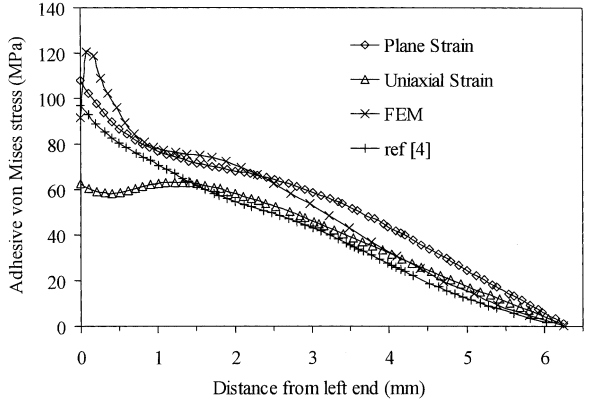

(b)

FIGURE 7 Adhesive stress and strain as a function of distance from the left end of the sandwich of Figure 5 for the present model, the model of Crocombe and Bigwood [4] and the finite element model. Plane strain ($\varepsilon_z = 0$) assumed in adhesive and adherends. (a) Peel and shear stress; (b) von Mises stress, which also shows curve for present model under uniaxial strain condition in adhesive ($\varepsilon_x = \varepsilon_z = 0$); (c) von Mises strain. (Continued)

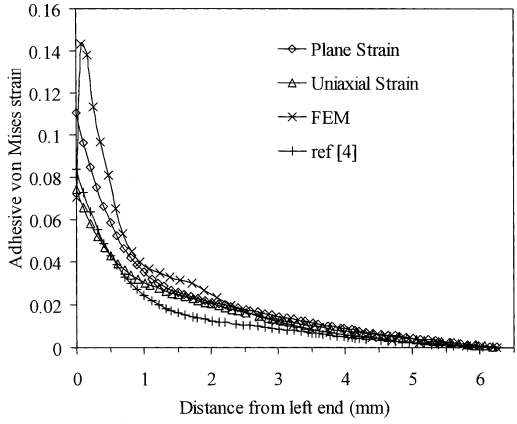

(c)

FIGURE 7 (Continued.)

Mises strain of the FEM and the uniaxial strain model are almost identical at the free edge of the sandwich where failure will occur first.

PEEL MODEL

The modified adhesive sandwich model described above was coupled to an existing model of the detached part of a flexible-to-rigid peel joint as illustrated in Figure 8. This was done to permit the use of experimental peel data in developing a suitable failure criterion for adhesive joints with adherends that undergo extensive plastic deformation. Following Moidu et al. [12], the detached strip to the left of the peel root was treated as an elasto-plastic slender beam in pure bending, and its curvature and rotation at the "root" (point of connection with the adhesive) were matched to those of the sandwich. From [12], the root curvature k_B, root rotation angle ϕ, and peel force F are related as

$$\frac{F}{bM_oK_e}[1-\cos(\theta-\phi)]=\frac{k_B^2}{3} \quad \text{for } 1<k_B\le\left(1+\frac{1}{1-\alpha}\right) \tag{30a}$$

$$\begin{aligned}\frac{F}{bM_oK_e}[1-\cos(\theta-\phi)]=&\frac{1}{3}\left[1-(1-\alpha)^3\right]k_B^2+\left[2(1-\alpha)^2-\alpha(1-\alpha)(2-\alpha)\right]k_B\\&+\frac{(2-\alpha)^2}{3k_B(1-\alpha)}\left[6(1-\alpha)-\left(4-\alpha^2\right)\right]+(2-\alpha)^2(1+\alpha)\\&-4(1-\alpha)(2-\alpha)\quad \text{for } k_B\ge\left(1+\frac{1}{1-\alpha}\right)\end{aligned} \tag{30b}$$

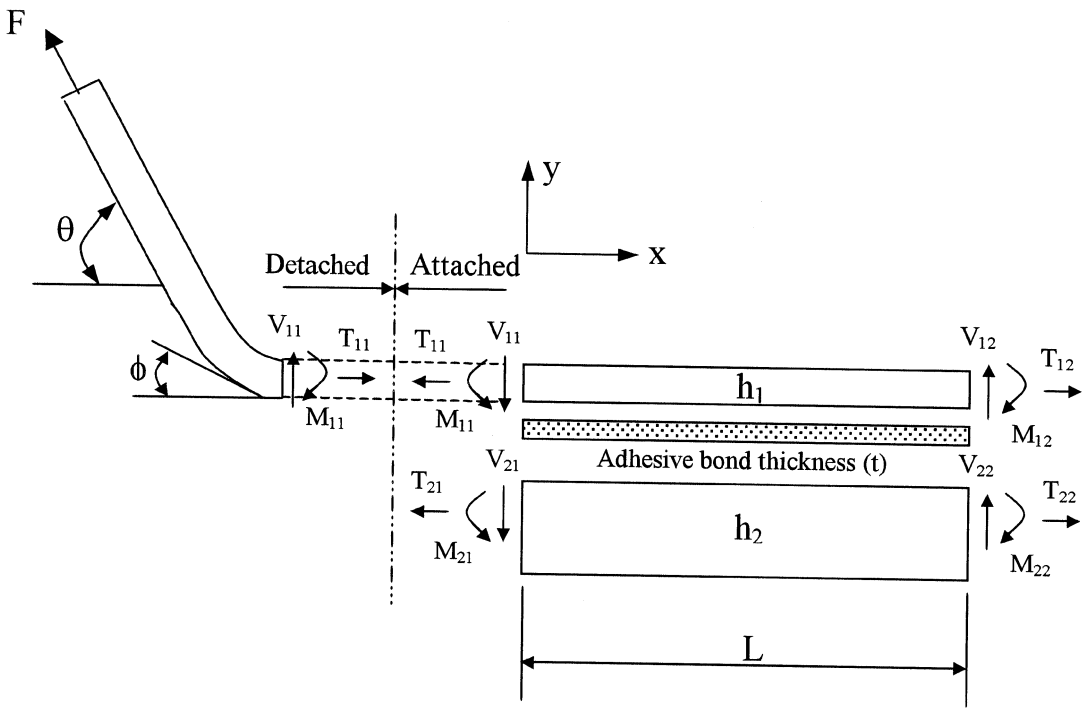

FIGURE 8 Decomposition of rigid-flexible peel specimen into an adhesive sandwich and a detached strip.

where M_o is the collapse moment, K_e is the elastic limit curvature, and α is the ratio of the bilinear adherend plastic modulus to the elastic modulus.

For flexible-to-rigid peel specimens (Figure 8)—assuming L is sufficiently large—the right-hand side boundary forces (T_{12}, V_{12}, $M_{12}, T_{22}, V_{22}, M_{22}$) in Figure 8 are all zero. The boundary forces on the left hand side are equal but in opposite directions for the top and bottom adherends:

$$T_{21} = -T_{11}; \quad V_{21} = -T_{11}; \quad M_{21} = -M_{11} \tag{31}$$

A simple force balance on the detached peel strip gives:

$$T_{11} = F \ \cos(\theta) \tag{32a}$$

$$V_{11} = -F \ \sin(\theta) \tag{32b}$$

The bending moment M_{11} is related to the maximum curvature k_B at the root as follows [13]:

$$M_{11} = -m_B M_o = -M_o \frac{2}{3} k_B \quad \text{if } k_B < 1 \tag{33a}$$

$$M_{11} = -m_B M_o = -M_o \left[(1-\alpha)\left(1 - \frac{1}{3k_B^2}\right) + \frac{2}{3}\alpha k_B \right] \quad \text{if } k_B \geq 1 \tag{33b}$$

Equations (30) to (33) imply that an additional implicit relationship can be established between k_B and ϕ, expressed as:

$$f(k_B, \phi) = 0 \tag{34}$$

Values of k_B and ϕ can be obtained by jointly solving Equations (30) and (34) numerically using the Newton-Raphson method. The flow chart for the overall solution procedure is shown in Figure 9.

Comparisons with Finite Element Model

In order to verify the new peel analysis, comparisons were made with a finite element model (ANSYS v. 5.7) [11]. The peel configuration used was a 1 mm thick AA5754-O aluminum strip (bilinear stress-strain properties: $E_{el} = 71\,\text{Gpa}$, $E_{pl} = 483\,\text{Mpa}$, $\sigma_y = 100\,\text{Mpa}$) bonded to a rigid base by an adhesive with the same properties as in the sandwich model of Figure 5. The elastic Poisson ratio for both adhesive and adherends was 0.37, while the plastic Poisson ratio for the adherends was 0.5. The plastic Poisson ratio for the adhesive was 0.5 in the finite element model and 0.47 in the analytical model. The peel force

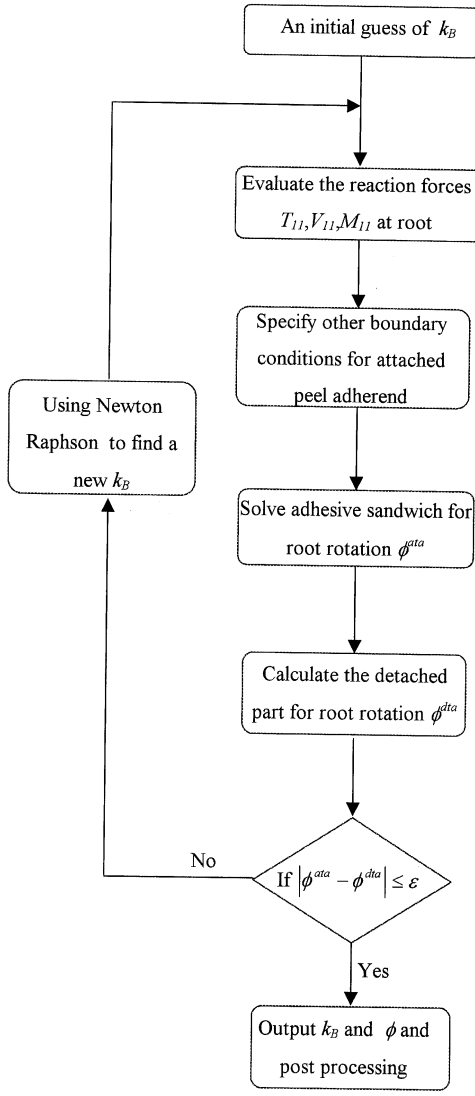

FIGURE 9 Flow chart of iterative solution procedure used in peel model.

$F = 14.7$ N/mm and the peel angle $\theta = 90°$. Figures 10a–c show the adhesive tensile, shear, and von Mises strain distributions as a function of distance from the peel root for the finite element model, the present model under plane strain conditions ($\varepsilon_z = 0$), and the present model under uniaxial strain ($\varepsilon_x = \varepsilon_z = 0$). The results for the latter

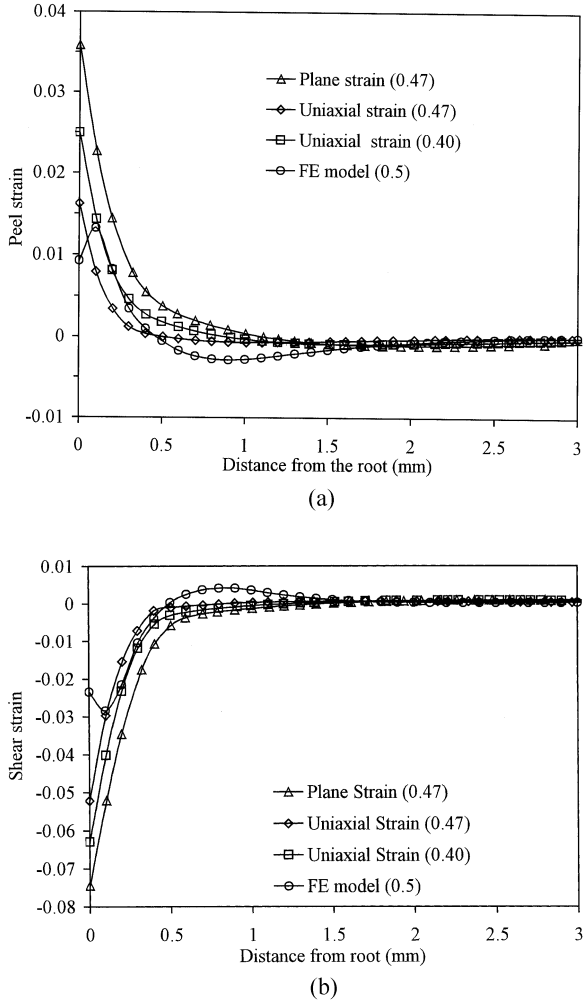

FIGURE 10 Adhesive strain as a function of distance from the peel root for plane strain ($\varepsilon_z = 0$) finite element model and present analytical model under 2 conditions: plane strain ($\varepsilon_z = 0$), and uniaxial strain ($\varepsilon_x = \varepsilon_z = 0$). Value of plastic Poisson ratio shown in brackets. Rigid-flexible peel geometry with adhesive properties as in Figure 5, 1 mm thick AA5754-O adherend peeled at 90°. (a) Peel (tensile) strain; (b) shear strain; (c) von Mises strain, finite element results shown for interface and midplane nodes. (Continued)

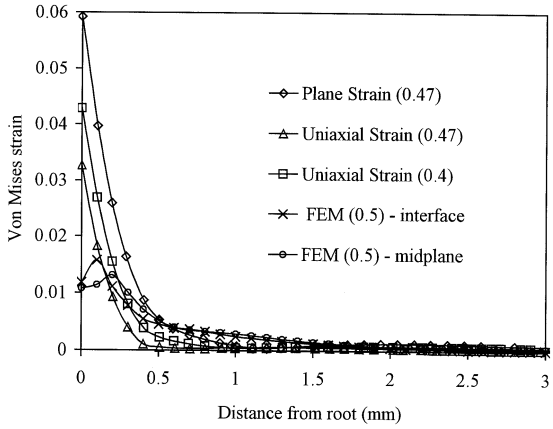

(c)

FIGURE 10 (Continued.)

model are also shown for an additional adhesive plastic Poisson ratio ($\upsilon_p = 0.4$). As with the earlier comparisons of the sandwich model (Figures 6 and 7), the discrepancy between the analytical models and the finite element model decreases with the distance from the peel root, becoming very small beyond 1 mm. The uniaxial strain model ($\upsilon_p = 0.47$) shows the best overall agreement with the finite element model because of its approximation of σ_x in the adhesive. It is seen that the peel strain predicted by this model is particularly sensitive to the choice of υ_p. As seen in Figures 6 and 7, the analytical model predicts that the adhesive strains are maximum at the root, while the finite element analysis shows extrema occurring very close to the root. Figure 10c shows the FEM von Mises strains at both the interface and midpoint nodes, illustrating the variation within the adhesive as a function of y.

Figures 11a–c show the adhesive tensile, shear, and von Mises strains, respectively, predicted by the model of Crocombe and Bigwood [4] and the present model with a plane strain ($\varepsilon_z = 0$) adhesive layer and the same peel case used in Figures 10a–c. The inclusion of shear deformation in the present model increases each type of strain significantly and leads to greater curvature at the peel root.

The internal consistency of the plane strain sandwich model was checked by comparing the work done by an external bending moment per unit width of 380 Nmm/mm applied to both ends of the sandwich (shown in Figure 5) with the total strain energy in the adherends and

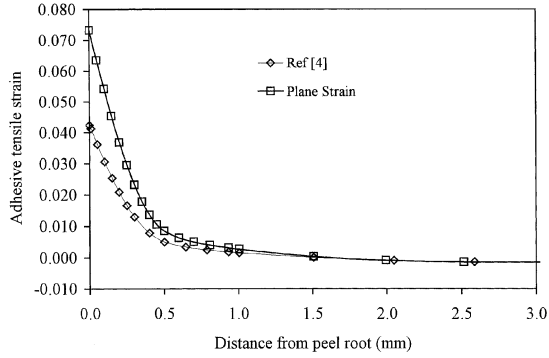

(a)

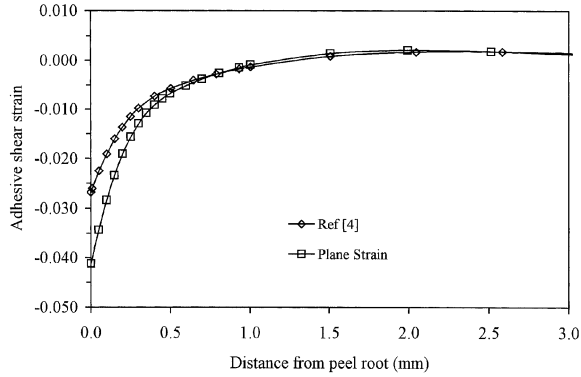

(b)

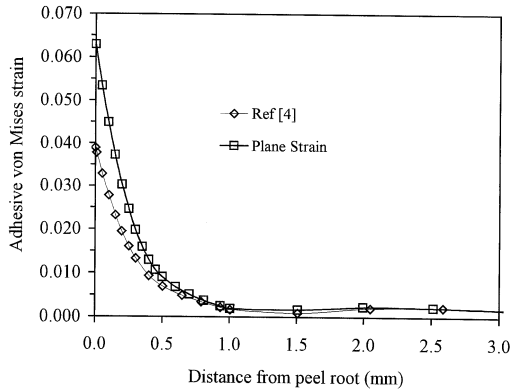

(c)

FIGURE 11 Adhesive strains predicted by model of Crocombe and Bigwood [4] and the present model with a plane strain adhesive and the rigid-flexible 90° peel case used in Figure 10. (a) Tensile (peel) strain; (b) shear strain; (c) von Mises strain.

adhesive. The moments caused a predicted rotation of 5.7° so that the total work done was 42.2 J/mm. The resulting strain energy stored in the adherends and adhesive was 32.4 J/mm and 8.4 J/mm, respectively, giving a total of 40.8 J/mm. Thus, the external work done matched the stored energy to within approximately 3%.

The practical utility of the present analytical model cannot be assessed solely by comparisons with finite element results. Although they give assurance that the analytical predictions of stress and strain are reasonable, the ultimate test is to obtain consistent correlations with experimental data using a single failure criterion. Only this test can determine whether the analytical model is sufficiently accurate to be of engineering use. This question is pursued in the accompanying article in this volume [5].

CONCLUSIONS

An existing analytical adhesive sandwich model [4] has been extended to include the effect of shear deformation in the adherends. A uniaxial strain condition ($\varepsilon_x = \varepsilon_z = 0$) was examined to provide a simple approximation of the longitudinal stress (σ_x) in the adhesive layer. This sandwich model can be a generic element in a wide variety of adhesive joint configurations. For example, in the present case, it has been coupled to an existing model for the detached strip of a peel specimen [12] to create a new model for the rigid-flexible peel geometry. This enabled the experimental verification of the sandwich model using peel data [5]. Both the sandwich and peel models predicted adhesive stress and strain distributions that captured the overall trends of the finite element model, but missed some of the localized phenomena near the free edge. In the accompanying article [5], experimental peel data are used with the present model to assess the applicability of a critical von Mises strain and a critical fracture energy failure criterion.

By allowing for any form of adherend and adhesive plastic behavior, the present peel model is less restrictive than earlier models, such as [12–15], that accommodated adherend yielding but assumed only an elastic adhesive response.

REFERENCES

[1] Fernlund, G., Papini, M., McCammond, D., and Spelt, J. K., *Composites Science and Tech.* **51**, 587–600 (1994).
[2] Papini, M., Fernlund, G., and Spelt, J. K., *Int. J. Adhesion and Adhesives* **14**, 5–13 (1994).
[3] Fernlund, G., and Spelt, J. K., *Composites Sci. and Tech.* **50**, 441–449 (1994).

[4] Crocombe, A. D., and Bigwood, D. A., *J. of Strain Analysis* **27**, 211–218 (1992).
[5] Wang, R., Sinclair, A. N., and Spelt, J. K., *J. Adhesion* **79**, 1–18 (2002).
[6] Wang, R., *Adhesive Failure with Adherend Yielding: Experiments and Models,* MASc Thesis, Department of Mechanical and Industrial Engineering, University of Toronto (2001).
[7] Timoshenko, S., *Mechanics of Materials* (Van Nostrand Reinhold Co., New York, 1972).
[8] Cpereyra, V., and Lentini, M., *Lecture Notes in Computer Science* (Springer-Verlag, Berlin, Heidelberg, New York 1979), pp. 67–87.
[9] Mattheij, R. M., and Russell, R. D., *Numerical Solution of Boundary Value Problems for Ordinary Differential Equations* (Society for Industrial and Applied Mathematics Philadelphia, 1995).
[10] *IMSL Math/Library Manual*, Chapter 5: Differential Equations-(Visual Numeric, Inc., Houston, 1997), pp. 641–689.
[11] Cui, J., *Finite Element Modeling of Adhesive Failure with Adherend Yielding*, MASc. Thesis, Department of Mechanical and Industrial Engineering, University of Toronto (2001).
[12] Moidu, A. K., Sinclair, A. N., and Spelt, J. K., *J. Testing and Evaluation* **26**, 247–254 (1998).
[13] Moidu, A. K., Sinclair, A. N., and Spelt, J. K., *J. Testing and Evaluation* **23**, 241–253 (1995).
[14] Kinloch, A. J., Lau, C. C., and Williams, J. G., *Int. J. Fracture* **66**, 45–70 (1994).
[15] Kim, K. S., and Kim, J., *J. Eng. Materials and Tech.* **110**, 266–273 (1988).

APPENDIX: SHEAR STRESS AT THE NEUTRAL AXIS AND ITS DISTRIBUTION ACROSS THE ADHEREND

The analysis of deformation due to shear under a general loading can be decomposed into two simple cases, as shown in Figure A1. Superposition of Case 1 and Case 2 gives the total shear stress at the neutral axis, as expressed by Equation (25) used above.

Case 1

If $M \leq M_{critical}$ such that the surfaces of the adherend remain elastic, then shear stress τ_{xy} can be calculated based on the parabolic distribution as

$$\tau_{xy} = -\frac{V}{2I}\left[\left(\frac{h}{2}\right)^2 - y^2\right] \quad \text{if } M \leq M_{critical} \tag{A1}$$

where I is the moment of inertia of the cross-section, and $M_{critical}$ can be calculated as

$$M_{critical} = \sigma_{yp,x} h^2/6 \tag{A2}$$

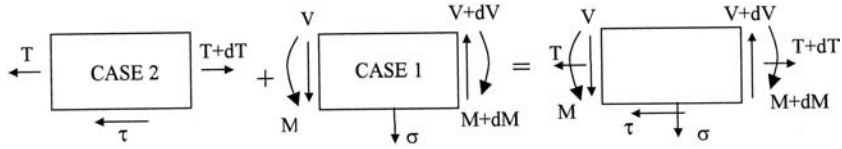

FIGURE A1 Superposition of shear stress and strain in adherends.

At the neutral axis

$$\tau_{neutral} = \tau_{\max} = -\frac{3}{2}\frac{V}{bh} = -AV \tag{A3}$$

where $A = \frac{3}{2bh}$.

If $M > M_{critical}$, which means the surfaces have yielded, then the calculation of the τ_{xy} distribution is rather complicated. However, as with the elastic case, τ_{xy} is maximum at the neutral axis and is given by

$$\tau_{neutral} = \tau_{\max} = -\frac{V\left[12(1-\alpha)+3\alpha h^2/r^2\right]}{16(1-\alpha)+2\alpha h^3/r^3} = -BV \tag{A4}$$

where $B = \frac{\left[12(1-\alpha)+3\alpha h^2/r^2\right]}{16r(1-\alpha)+2\alpha h^3/r^2}$, $\alpha = \frac{E_{pl\,x}}{E_{el\,x}}$, the ratio of the longitudinal plastic modulus to the longitudinal elastic modulus of the adherend, and r is the distance to the neutral axis from the location of the onset of yielding in the adherend, which can be found by solving the following polynomial equation:

$$\sigma_{yp,x}\left[\frac{h^2}{2}(1-\alpha)+\frac{1}{12}\frac{\alpha}{r}h^3-\frac{1}{3}r^2(1-\alpha)\right]-M=0 \tag{A5}$$

Case 2

The calculation of shear stress τ_{xy} due to tension requires a known σ_x distribution across the section resulting from the tensile force T. However, due to the nature of the bilinear adherend material property, it is very complicated to obtain the exact distribution of σ_x. Therefore, an assumption of uniform distribution is applied here, which leads to an average shear stress given by

$$\tau_{neutral} = \tau_{average} = \frac{1}{h}\int_{-h/2}^{h/2}\tau_{xy}\,dy = \frac{1}{2}\tau_a \tag{A6}$$

where τ_a is the shear stress of the adherend at the adhesive interface.